Polariton bunching and anti-bunching in a photonic dot controlled by a magnetic field

Yongyou Zhang and Guojun Jin*

National Laboratory of Solid State Microstructures and Department of Physics, Nanjing University, Nanjing 210093, China

(Received 23 January 2009; revised manuscript received 8 April 2009; published 1 May 2009)

Using the Liouville–von Neumann equation, we study the polarization dynamics of the polaritons localized in a photonic dot excited by continuous-wave (cw) or pulse laser beams. Pumped by the cw and circularly polarized laser, in the weak magnetic-field region we find a strong polariton anti-bunching and a platform behavior in the variation in the polariton occupation with the pump field, and the latter manifestly displays the polariton quantum blockade. In the case of using the cw and linearly polarized laser, we find the redshift of the polariton energy in the polariton magnetic spectrums, due to the effective-attractive interaction between the polaritons with antiparallel spins; moreover the polaritons with antiparallel spins are always anti-bunching in the low excitation regime. Especially, we demonstrate the single-photon character of the photonic dot in the excitation of the pulsed wave and linearly polarized laser, and the emitted-photon polarization can be conveniently adjusted by an applied magnetic field.

DOI: 10.1103/PhysRevB.79.195304 PACS number(s): 42.50.−p, 71.36.+c, 03.67.−a, 42.55.Sa

I. INTRODUCTION

Semiconductor microcavities with embedded quantum wells have become an attractive field for theoretical and experimental physicists, due to their unusual light-matter interacting effects. The quantum-well excitons and cavity photons can be coupled to form the mixed modes—exciton polaritons—which have abundant physics. Therefore, semiconductor microcavities have huge potential applications such as optical amplifiers,[1–3] lasers,[4–6] optical switchers,[7] and optical gates.[8] Meanwhile, semiconductor microcavities also provide many interesting questions in fundamental physics such as Bose-Einstein condensation[9–11] and energy-band structure.[12] The exciton polaritons have been studied in many experiments from the strong to weak exciton-photon coupling regimes.[1–3,13,14] Especially, the angle-resonant experiment[1] displayed a giant optical nonlinearity which was well described by an enlightening three-level model.[15,16] The polarization-dependent dynamics of the polariton-polariton scattering have also been studied in detail in many pump-probe configurations.[17–22] Technically, semiconductor microcavities can be lithographed and etched into transverse size of magnitude about from 0.1 to 1.0 μm. In such small structures, also alternatively called the photonic dots,[5,23,24] the in-cavity photons are confined in three directions. Thus, the photonic dots have attracted many researchers to study the localized polaritons.[25,26] So far, most of the photonic dots are fabricated by the GaAs/AlGaAs semiconductors; therefore we will take the parameters of the GaAs/AlGaAs photonic dots in this work.

The progress of quantum communication[27] and quantum information[28] has been founded on the quantum properties of electromagnetic fields, and one key device is the single-photon emitter. Generally, the single-photon emitter can be obtained by using the parametric down-conversion process of bulk nonlinear crystals,[28] attenuated lasers, semiconductor electric quantum dots,[29–32] or colored centers in diamond nanocrystals.[33] It has been theoretically suggested that the photonic dot strongly coupled to the embedded quantum well can also be used to achieve the single-photon emission,[25] due to the effective repulsive interactions between the quantum-well excitons with parallel spins. Here we would follow its formulation and extend to consider the magnetic-field-modulated polariton bunching and anti-bunching, as well as the single-photon emission. On the other hand, the polarization steps are recently studied in the equilibrium thermal polaritons localized in the photonic dots.[26] Because the effective interaction between the polaritons with antiparallel spins is attractive, the polaritons in the semiconductor microcavities prefer being linearly polarized,[10,34] which obviously can be disturbed by applied magnetic field.[26] Experimentally, the magnetic-field effects have been studied in detail on the linear optical response of the polaritons.[35,36]

For the polaritons localized in a photonic dot, the polarization dynamics has not been well studied under an applied magnetic field, although it can be expected that the polarization dynamics may strongly influence the polariton application to the single-photon emitter. Therefore, in this work we will mainly focus our attention on the polariton bunching and anti-bunching affected by the polariton polarization dynamics. It is reasonable to assume that the polaritons in the photonic dot behave like ideal bosons and the magnetic field is applied along the structure-grown axis. For simplicity, we can further neglect the Landau quantization of electrons and holes[37] because it is not important to the polarization dynamics of the polaritons.[26] The effect of the magnetic field is taken into account only by introducing the exciton Zeeman energy.

The paper is organized as follows. In Sec. II, we derive the rotating-wave Hamiltonian for the lower-branch polariton and introduce the Liouville–von Neumann equation to describe the polariton polarization dynamics. In Sec. III the numerical results are obtained and discussed in several pump geometries. Finally, the conclusion of this work is summarized in Sec. IV.

II. THEORETICAL FORMULATION

In the system of a photonic dot with spatial confinement, we can consider only the dynamics of the fundamental pho-

tonic mode strongly coupled to the certain excitonic level of the quantum well, and the corresponding Hamiltonian is

$$\mathcal{H} = \sum_{\sigma} \left\{ [E_C a_\sigma^\dagger a_\sigma + \Omega_R (a_\sigma^\dagger b_\sigma + b_\sigma^\dagger a_\sigma) + (E_X - \eta_\sigma \Omega_B) b_\sigma^\dagger b_\sigma] + \frac{1}{2} \sum_{\sigma'} V_{\sigma\sigma'} b_\sigma^\dagger b_{\sigma'}^\dagger b_{\sigma'} b_\sigma + f_\sigma(t) e^{-i\omega_P t} a_\sigma^\dagger + f_\sigma^*(t) e^{i\omega_P t} a_\sigma \right\}, \tag{1}$$

where $E_{C(X)}$, $a_\sigma^\dagger(b_\sigma^\dagger)$, and $a_\sigma(b_\sigma)$ represent the energy, the creation, and annihilation operators of the photonic (excitonic) mode with spin $\sigma(=\uparrow,\downarrow)$, respectively. Ω_R is the Rabi splitting and $\Omega_B = g_X \mu_B B$ is the exciton Zeeman energy, with g_X being the exciton g factor, μ_B is the Bohr magneton, and B is the external field. Although g_X depends on the material and structure, it is associated with the magnetic field B, so we can take Ω_B as the single parameter directly in the study. The detuning $\Delta_{\sigma B} = E_C - E_X + \eta_\sigma \Omega_B$ depends on Ω_B, and η_σ is defined as $\eta_\uparrow = 1$ and $\eta_\downarrow = -1$. $V_{\sigma\sigma'}$ represents the nonlinear interaction between the excitons with spin σ and σ', and $V_{\uparrow\uparrow} = V_{\downarrow\downarrow}$ and $V_{\uparrow\downarrow} = V_{\downarrow\uparrow}$ hold. Finally, $f_\sigma(t)$ describes the σ-polarized component of the excitation field[15,16] and has the form

$$f_\uparrow(t) = |f_P(t)| \cos\theta, \quad f_\downarrow(t) = |f_P(t)| \sin\theta, \tag{2}$$

where $|f_P(t)|$ represents the amplitude of the applied excitation field with frequency ω_P and the circular polarization degree $\lambda_P = \cos(2\theta)$ is defined. In the following, we will mainly focus on the circularly and linearly polarized excitations which correspond to $\lambda_P = 1(\theta = 0)$ and $\lambda_P = 0(\theta = \pi/4)$, respectively.

In order to study the polariton polarization dynamics directly, we convert the photon and exciton operators (a_σ, b_σ) into the lower and upper polariton operators $(P_{L\sigma}, P_{U\sigma})$ by the transformations

$$P_{L\sigma} = C_{L\sigma} a_\sigma + X_{L\sigma} b_\sigma, \quad P_{U\sigma} = C_{U\sigma} a_\sigma + X_{U\sigma} b_\sigma. \tag{3}$$

By the canonical properties of these operators, we have $C_{U\sigma} = X_{L\sigma}$, $X_{U\sigma} = -C_{L\sigma}$, and

$$X_{L\sigma} = \Omega_R / \sqrt{(\mathcal{E}_{L\sigma} - E_X + \eta_\sigma \Omega_B)^2 + \Omega_R^2},$$

$$C_{L\sigma} = (\mathcal{E}_{L\sigma} - E_X + \eta_\sigma \Omega_B) / \sqrt{(\mathcal{E}_{L\sigma} - E_X + \eta_\sigma \Omega_B)^2 + \Omega_R^2}, \tag{4b}$$

where

$$\mathcal{E}_{L\sigma} = \frac{1}{2} [E_C + E_X - \eta_\sigma \Omega_B - \sqrt{\Delta_{\sigma B}^2 + 4\Omega_R^2}] \tag{5}$$

represents the energy of the lower-polariton branch with spin σ. As a typical example, we can show the magnetic-field-dependent energy of the lower polaritons plotted in Fig. 1(a). The following parameters of the typical GaAs-AlGaAs photonic dots are used in Fig. 1 and throughout this work, namely, $E_X = E_C = 0$, $\Omega_R = 2.5$ meV, $\hbar\gamma_\uparrow = \hbar\gamma_\downarrow = 0.1$ meV,[25] $\mathcal{G}_{\uparrow\uparrow}(\Omega_B = 0) = \mathcal{G}_{\downarrow\downarrow}(\Omega_B = 0) = 4.8$ meV, and $\mathcal{G}_{\uparrow\downarrow}(\Omega_B = 0) = -0.48$ meV.[26]

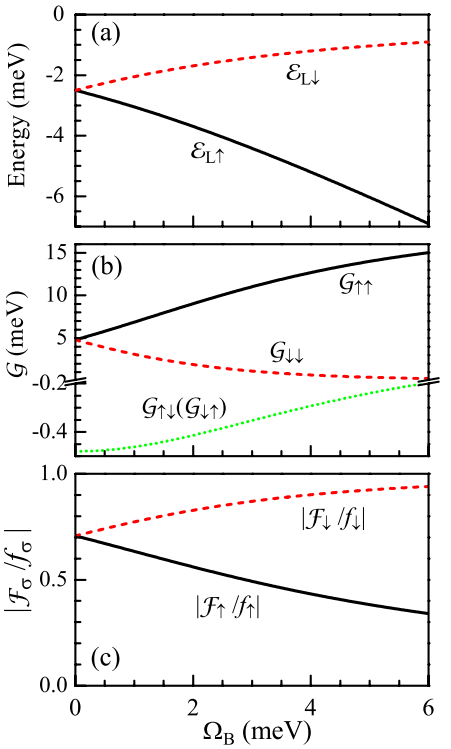

FIG. 1. (Color online) Dependences of the (a) polariton energies, (b) nonlinear interactions, and normalized pump fields on magnetic field.

We are interested in the dynamics of the lower polaritons. From Eqs. (1) and (3) we can obtain the effective Hamiltonian for the lower polaritons, i.e.,

$$\mathcal{H}_{\mathrm{LP}} = \sum_{\sigma} \mathcal{E}_\sigma P_\sigma^\dagger P_\sigma + \frac{1}{2} \sum_{\sigma\sigma'} \mathcal{G}_{\sigma\sigma'} P_\sigma^\dagger P_{\sigma'}^\dagger P_{\sigma'} P_\sigma + \sum_{\sigma} [\mathcal{F}_\sigma(t) e^{-i\omega_P t} P_\sigma^\dagger + \mathcal{F}_\sigma^*(t) e^{i\omega_P t} P_\sigma], \tag{6}$$

where $\mathcal{G}_{\sigma\sigma'} = X_{L\sigma}^2 X_{L\sigma'}^2 V_{\sigma\sigma'}$, $\mathcal{F}_\sigma(t) = C_{L\sigma} f_\sigma(t)$, and for easy writing we have omitted the subscript L in $\mathcal{E}_\sigma$, $P_\sigma^\dagger$, and P_σ. It is obvious that $\mathcal{G}_{\uparrow\downarrow} = \mathcal{G}_{\downarrow\uparrow}$, and the variations of $\mathcal{G}$ and $|\mathcal{F}_\sigma / f_\sigma|$ with Ω_B are shown in Figs. 1(b) and 1(c), respectively. From Fig. 1(b), we can see that both $\mathcal{G}_{\uparrow\uparrow}$ and $|\mathcal{G}_{\uparrow\downarrow}|$ increase, yet $\mathcal{G}_{\downarrow\downarrow}$ decreases with Ω_B; all these curves indicate that the polariton characters can be controlled by changing the magnetic field. In addition, the pump term $\mathcal{F}_\sigma(t)$ also depends on Ω_B through the Hopfield coefficient $C_{L\sigma}$. Simply speaking, because of the dependence of the detuning $\Delta_{\sigma B}$ on the magnetic field, all the parameters in Eq. (6) are dependent on the magnetic field.

For studying the quantum behavior of the lower polaritons, it is convenient to work in the rotating frame,[25] and thus we make the following transformation for $\mathcal{H}_{\mathrm{LP}}$ to obtain the rotating-frame Hamiltonian $\tilde{\mathcal{H}}_{\mathrm{LP}}$, namely,

$$\tilde{\mathcal{H}}_{\mathrm{LP}} = R^\dagger(t) \mathcal{H}_{\mathrm{LP}} R(t) - i\hbar R^\dagger(t) \frac{\partial}{\partial t} R(t), \tag{7}$$

where $R(t) = e^{-i\omega_P t(P_\uparrow^\dagger P_\uparrow + P_\downarrow^\dagger P_\downarrow)}$. Substituting Eq. (6) into Eq. (7), we have

$$\tilde{\mathcal{H}}_{\mathrm{LP}} = \sum_{\sigma} \Delta\mathcal{E}_{\sigma} P_{\sigma}^{\dagger} P_{\sigma} + \frac{1}{2} \sum_{\sigma\sigma'} \mathcal{G}_{\sigma\sigma'} P_{\sigma}^{\dagger} P_{\sigma'}^{\dagger} P_{\sigma'} P_{\sigma} + \sum_{\sigma} [\mathcal{F}_{\sigma}(t) P_{\sigma}^{\dagger} + \mathcal{F}_{\sigma}^{*}(t) P_{\sigma}], \tag{8}$$

where $\Delta\mathcal{E}_{\sigma}=\mathcal{E}_{\sigma}-\omega_P$. Naturally, the quantum dynamics of the lower polaritons can be studied by the rotating-frame density matrix $\tilde{\rho}=R^{\dagger}(t)\rho R(t)$, which is determined by the Liouville–von Neumann equation

$$i\hbar \frac{d}{dt}\tilde{\rho} = [\tilde{\mathcal{H}}_{\mathrm{LP}}, \tilde{\rho}] + iD\tilde{\rho}. \tag{9}$$

Here $D\tilde{\rho}$ represents the dissipation operator accounting for the losses of the microcavity and has the form

$$D\tilde{\rho} = \sum_{\sigma} \gamma_{\sigma}([P_{\sigma}\tilde{\rho}, P_{\sigma}^{\dagger}] + [P_{\sigma}, \tilde{\rho} P_{\sigma}^{\dagger}]), \tag{10}$$

where $\gamma_{\sigma}=X_{L\sigma}^2\gamma_X+C_{L\sigma}^2\gamma_C$ represents the homogeneous linewidth of the lower polaritons, with γ_X and γ_C being the homogeneous linewidth of the excitonic and photonic modes. For the sake of simplicity, we assume $\gamma_X=\gamma_C$, therefore the polariton linewidth γ_{σ} could be treated as independent of the magnetic field, as done in our following calculations. It is convenient for us to expand the density operator $\tilde{\rho}$ in the Fork basis, i.e.,

$$\tilde{\rho} = \sum_{n_{\uparrow}n_{\downarrow}n'_{\uparrow}n'_{\downarrow}} \tilde{\rho}_{n_{\uparrow}n_{\downarrow}n'_{\uparrow}n'_{\downarrow}} |n_{\uparrow}, n_{\downarrow}\rangle\langle n'_{\uparrow}, n'_{\downarrow}|. \tag{11}$$

Then, substituting Eq. (11) into Eq. (9), the dynamic equations for the density-matrix elements $\tilde{\rho}_{n_{\uparrow}n_{\downarrow}n'_{\uparrow}n'_{\downarrow}}$ will be obtained, and with the initial polariton state, such as the vacuum state, the polarization dynamics of the polaritons will be fully determined.

Using the density matrix, we can easily get the occupation number of the lower polaritons, that is,

$$\mathcal{N}_{\sigma}(t) = \mathrm{Tr}[P_{\sigma}\tilde{\rho}(t)P_{\sigma}^{\dagger}] = \sum_{n_{\uparrow}n_{\downarrow}} n_{\sigma}\tilde{\rho}_{n_{\uparrow}n_{\downarrow}n_{\uparrow}n_{\downarrow}}, \tag{12}$$

and the two-time second-order correlation function,

$$G_{\sigma\sigma'}^{(2)}(t,t') = \mathrm{Tr}\{P_{\sigma}\mathcal{U}_{tt'}[P_{\sigma'}\tilde{\rho}(t')P_{\sigma'}^{\dagger}]P_{\sigma}^{\dagger}\}, \tag{13a}$$

$$g_{\sigma\sigma'}^{(2)}(t,t') = G_{\sigma\sigma'}^{(2)}(t,t')/[\mathcal{N}_{\sigma}(t)\mathcal{N}_{\sigma'}(t')], \tag{13b}$$

where $\mathcal{U}_{tt'}$ represents the evolution superoperator of the Liouville–von Neumann (9), and satisfies $\mathcal{U}_{tt}=1$. For convenience, we denote the equal-time second-order correlation function as $g_{\sigma\sigma'}^{(2)}(0)=g_{\sigma\sigma'}^{(2)}(t,t)$ in the following.

III. NUMERICAL RESULTS AND DISCUSSION

For clearly displaying the effects of a magnetic field on the polariton polarization, this section will be divided into three parts according to the pump-field types. They are (A) circularly polarized and continuous-wave (cw) excitation, (B) linearly polarized and cw excitation, and (C) linearly polarized and pulsed wave excitation. The Adams-Bashforth-Moulton method[38] is used to solve Eq. (9) to obtain the occupation number and correlation function. Such method is based on the multistep and the predictor-corrector technologies and so holds high efficiency and precision. In addition, we have considered the particle states $|n_{\uparrow},n_{\downarrow}\rangle$ up to $n_{\uparrow}=n_{\downarrow}=10$ in the calculation, and this cut-off approximation has well satisfied the numerical precision seen from the results.

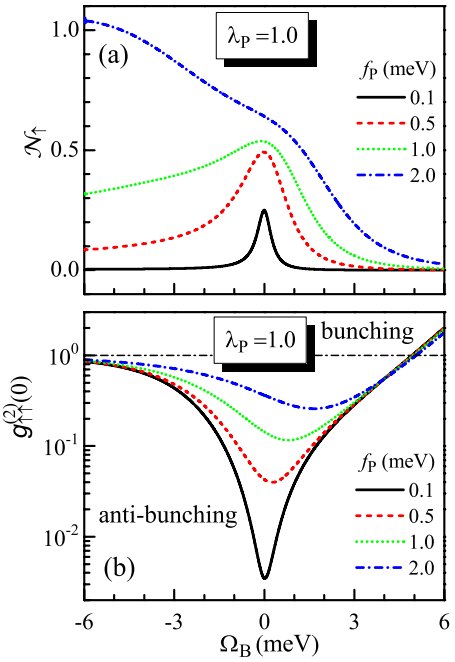

FIG. 2. (Color online) Variation in the (a) occupation number $\mathcal{N}_{\uparrow}$ and (b) equal-time correlation function $g_{\uparrow\uparrow}^{(2)}(0)$ with the magnetic field in steady states pumped by several cw lasers. Here $\lambda_P=1.0$ and $\omega_P=\mathcal{E}_{L\uparrow}(\Omega_B=0)$.

A. Circularly polarized and cw excitation

Figure 2(a) shows the magnetic spectrum of the lower polaritons under several pump fields with $\lambda_P=1$. In this kind of excitations, we only need to consider the spin-up polaritons, for the spin-down polariton is not excited. Because we set $\omega_P=\mathcal{E}_{\uparrow}(\Omega_B=0)$, the resonant excitations occur at $\Omega_B=0$. Referred to the three lower curves in Fig. 2(a), such resonant peaks obviously do not shift with the pump intensity, which is due to that the polaritons mainly occupy the single-polariton state and the contribution of the multipolariton states can be neglected. It has known that the blueshift of the polariton energy comes from the repulsive interactions between the polaritons with parallel spins and increases with the pump field. Moreover, the corresponding nonlinear terms in Eq. (8) do not generate influence when they operate on the single-polariton state. Therefore, if the single-polariton state dominates in the photonic-dot system, the resonant peaks in the magnetic spectrums will not shift, such as the three lower curves in Fig. 2(a). The resonant-peak shift shall be expected as the pump field becomes strong enough. But, because the resonant peak can be shielded by the dependence of $\mathcal{F}_{\uparrow}$ on

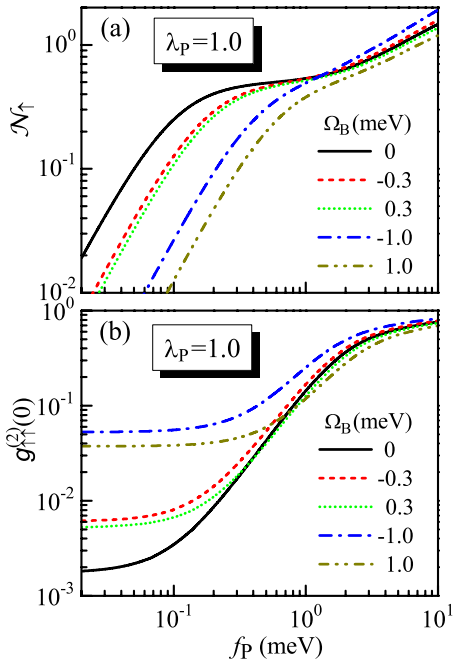

FIG. 3. (Color online) Variation of $\mathcal{N}_\uparrow$ and $g^{(2)}_{\uparrow\uparrow}(0)$ with the pump field f_P. Here $\lambda_P=1.0$ and $\omega_P=\mathcal{E}_{L\uparrow}(\Omega_B=0)$ such as in Fig. 2.

Ω_B, it is still difficult to observe the resonant-peak shift referred to the top curve of $f_P=2.0$ meV in Fig. 2(a). Clearly, the asymmetry of the magnetic spectrum is also attributed to the dependence of $\mathcal{F}_\uparrow$ on Ω_B.

The variation of $g^{(2)}_{\uparrow\uparrow}(0)$ with Ω_B is plotted in Fig. 2(b). In the region of $|\Omega_B|\lesssim 1$ meV, $g^{(2)}_{\uparrow\uparrow}(0)\ll 1$, implying the polariton anti-bunching. The effective repulsive interaction $\mathcal{G}_{\uparrow\uparrow}$ can induce the blueshift of the polariton energy and inhibits more-polariton injecting into the photonic dot, which is the so-called polariton quantum blockade. Particularly, for the low pump case (e.g., $f_P=0.1$ meV), $g^{(2)}_{\uparrow\uparrow}(0)\approx 0$ as $\Omega_B\sim 0$. Hence the polariton quantum blockade works well in this situation. However, as $|\Omega_B|\gtrsim 3$ meV, $g^{(2)}_{\uparrow\uparrow}(0)$ approaches to or even exceeds 1, implying that the polariton bunching appears owing to the nonresonant excitation. Simply speaking, the polaritons are better anti-bunching in the resonant excitation situation,[25] and such anti-bunching can be broken by the applied magnetic field. In addition, in the near resonant pump region (i.e., $\Omega_B\sim 0$), we can clearly see that $g^{(2)}_{\uparrow\uparrow}(0)$ sharply increases with the pump field f_P. In order to more clearly reveal this, we plot the variation of $\mathcal{N}_\uparrow$ and $g^{(2)}_{\uparrow\uparrow}(0)$ with the pump field under several magnetic fields in Figs. 3(a) and 3(b), respectively.

It is plain that all the curves in Fig. 3(a) satisfy $\log(\mathcal{N}_\uparrow)\propto\log(f_P)$ no matter in low or high excitation regimes, only with different proportional coefficients. This is due to that the photonic-dot loss and nonlinear interaction terms play major roles in the low and high excitation regimes, respectively. Importantly, the platform behavior in the curves of $\Omega_B=0$ and ± 0.3 meV in Fig. 3(a) is the pure quantum phenomenon and manifestly demonstrates the polariton quantum blockade. Thus, the repulsive interaction strongly inhibits the polariton increase in the platform region. Naturally, the platform behavior can be overcome by the high enough pump field, so does the polariton quantum blockade referred to Fig. 3(b). Strictly speaking, the polariton quantum blockade just takes effect in the platform region of $\mathcal{N}_\uparrow$ because the nonlinear interaction terms in Eq. (8) can be neglected in the low excitation regime, and thus the polariton dynamics is independent of the nonlinear interaction terms. But if specifying the polariton quantum blockade simply by $g^{(2)}_{\uparrow\uparrow}(0)<1$,[25] we can generally say that the polariton quantum blockade only works well in the low excitation regime. Due to the dependence of the detuning $|\Delta_{\uparrow B}|$ on $|\Omega_B|$, the platform behaviors become weaker and weaker with increasing $|\Omega_B|$. Meanwhile, the correlation function $g^{(2)}_{\uparrow\uparrow}(0)$ is evidently influenced by Ω_B, especially in the low excitation regime. Thus the magnetic field can conveniently be used to change the polariton-bunching character. Moreover, the dependence of $\mathcal{F}_\uparrow$ on Ω_B leads to the difference between the cases of $\pm|\Omega_B|$ in Figs. 3(a) and 3(b).

B. Linearly polarized and cw excitation

The above discussion has been focused on the circularly polarized excitation which is independent of the polarization dynamics. In order to study the polarization dynamics of polaritons, the pump field is set to be linearly polarized, i.e., $\lambda_P=0$, in this section. For this aim, we introduce the polarization degree for the polaritons defined as

$$\lambda_{\mathrm{LP}}=\frac{\mathcal{N}_\uparrow-\mathcal{N}_\downarrow}{\mathcal{N}_\uparrow+\mathcal{N}_\downarrow}. \tag{14}$$

Notice that when $\lambda_P=0$, the rotating-frame Hamiltonian in Eq. (8) is invariant under the transformation of $(\Omega_B,\sigma)\Leftrightarrow(-\Omega_B,\bar{\sigma})$. Thus the occupations $\mathcal{N}_\uparrow$ and $\mathcal{N}_\downarrow$ are symmetric with respect to the zero magnetic field, i.e., $\Omega_B=0$, as shown in Figs. 4(a) and 4(b). Apparently, the polarization degree λ_{LP} is centrosymmetric, as shown in Fig. 4(c). In common view, due to $\mathcal{G}_{\sigma\sigma}\gg|\mathcal{G}_{\sigma\bar{\sigma}}|$, the energy $\mathcal{E}_{L\uparrow}(\mathcal{E}_{L\downarrow})$ should be blue shifted with increasing the pump field f_P. But from Fig. 4(a), we see that the resonant peak of $\mathcal{N}_\uparrow$ shifts leftward with increasing f_P. Besides the polariton energy $\mathcal{E}_{L\uparrow}$ decreases with Ω_B, therefore, it is red shifted with increasing f_P. Consistent results for $\mathcal{E}_{L\downarrow}$ can be obtained by analyzing Fig. 4(b). As indicated in Sec. III A, the nonlinear interactions in Eq. (8) do not generate effect when they operate on the vacuum or single-polariton states. Based on the polariton occupations shown in Figs. 4(a) and 4(b), we can estimate that the number states playing major roles are the vacuum, single-polariton, and double-polariton states. Obviously, the states $|2,0\rangle$ and $|0,2\rangle$ cause blueshift for spin-up and spin-down polaritons, respectively, and the state $|1,1\rangle$ induces redshift for both them. Then, from Figs. 4(d)–4(f) we can find that $g^{(2)}_{\uparrow\downarrow}(0)>g^{(2)}_{\uparrow\uparrow(\downarrow\downarrow)}(0)$ as $|\Omega_B|\lesssim 1$ meV. Hence, the state $|1,1\rangle$ dominates among the three double-polariton states, and thus the polariton energies will be red shifted. As the three- or more-polariton states must be taken into account, such a red-shifted phenomenon could be weakened due to $\mathcal{G}_{\sigma\sigma}\gg|\mathcal{G}_{\sigma\bar{\sigma}}|$. But it is still difficult to observe the energy blueshift in the polariton magnetic spectrum because the resonant peak of the magnetic spectrum can be shielded by

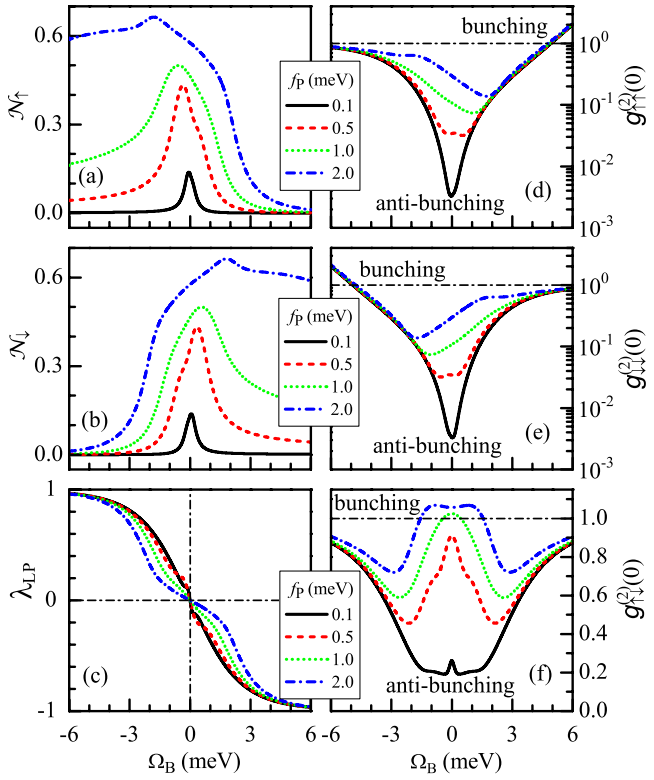

FIG. 4. (Color online) Variations in the polariton occupations, polarization degree, and equal-time correlation functions with the magnetic field. Here $\lambda_P=0$ and $\omega_P=\mathcal{E}_{L\uparrow(\downarrow)}(\Omega_B=0)$.

the dependence of $\mathcal{F}_\sigma$ on Ω_B. This is similar to the corresponding discussion in Sec. III A.

Considering the symmetry of the system in the case of the linearly polarized pump, it is natural that the polariton polarization is also linearly polarized when $\Omega_B=0$. As $|\Omega_B|\lesssim 1$ meV, due to the attractive interaction $\mathcal{G}_{\uparrow\downarrow}$ between the antiparallel polaritons, the polaritons prefer to be linearly polarized and thus the variation in the polarization λ_{LP} with Ω_B becomes flatter and flatter with increasing f_P, as shown in Fig. 4(c). This phenomenon can also be manifested by the relative relation $g^{(2)}_{\uparrow\downarrow}(0)\gg g^{(2)}_{\uparrow\uparrow(\downarrow\downarrow)}(0)$ referred to in Figs. 4(d)–4(f). When $|\Omega_B|\gtrsim 3$ meV, the polariton-energy shift and pump-term variation due to the magnetic field play major roles, thus the polaritons are prone to be circularly polarized. Therefore, it can be proved that the magnetic field can be used to efficiently adjust the polariton polarization in the photonic-dot system. As shown in Figs. 4(d) and 4(e), as $|\Omega_B|\gtrsim 3$ meV $g^{(2)}_{\sigma\sigma}(0)$ approaches to or exceeds 1, implying the bunching of the polaritons with parallel spins, which is similar to the circularly polarized and cw excitation. Differently, in Fig. 4(f) the equal-time correlation function $g^{(2)}_{\uparrow\downarrow}(0)$ indicates that the polaritons with antiparallel spins are always anti-bunching in the low excitation regime, and with increasing the pump field, they transit into bunching in the central range of $|\Omega_B|$. This is due to that the probabilities of multipolariton states are rather small whether in the low excitation regime or in the strong magnetic-field situation.

From the above discussion, we find that the polaritons can be strongly polarized by the magnetic field Ω_B in the excitation situation of the linearly polarized pump. In this polarized pump case, the magnetic field and pump intensity play major roles in the polariton bunching and anti-bunching. On the other hand, from Sec. III A, we have known that the polariton polarization is independent of the magnetic field when the pump field is purely circularly polarized, i.e., λ_{LP} equals ± 1 as $\lambda_P=\pm 1$, no matter what values of Ω_B. Thus, it is natural to expect that the linearly polarized pump field can be used to achieve the single-photon emitter whose emitted-photon polarization can be adjusted by the magnetic field.

C. Linearly polarized and pulsed wave excitation

It is known that for a single-photon emitter, the pump excitation should be the pulsed wave; thus in this section we use the pulsed laser as the excitation source to investigate the characters of the single-photon emitter structured by the photonic dot. According to Figs. 3(a) and 4(f), the amplitude of the pulse pump term $f_P(t)$ had better be smaller than 0.5 meV, and thus we take 0.3 meV as an example to study and state the single-particle character of the polaritons.

When $\Omega_B=0$, it is obvious that the polariton system is symmetric with respect to the polariton spin; thus the spin-up and spin-down polaritons have the same occupations, as plotted in Fig. 5(a). But its excitation is nonresonant [the pump frequency is set to be $\omega_P=\mathcal{E}_{L\uparrow}(\Omega_B=2$ meV)], therefore, the polariton occupations are smaller than the resonant excitation cases such as the thick solid line in Fig. 5(c). In Fig. 5(b), we plot the time-dependent correlation functions $G^{(2)}_{\sigma\sigma'}(t,t')$ which have been renormalized to their maximums, respectively. Due to the symmetry of Eq. (8), the shapes of the four correlation functions are the same. The depletion of the central peaks indicates that no matter what the polariton spin is, the polaritons are always anti-bunching, which just demonstrates the single-photon character. Obviously, we are interested in the polariton anti-bunching here, and similarly, the photon anti-bunching can be achieved in a quantum dot single-photon turnstile device.[32] In fact, the polariton bunching has been observed in the planar semiconductor microcavities.[9] In one word, in the case of $\Omega_B=0$ the photons emitted from the photonic dot are linearly polarized and hold the single-particle character.

In Figs. 5(c) and 5(d), we set $\Omega_B=2$ meV and $\omega_P=\mathcal{E}_{L\uparrow}(\Omega_B=2$ meV); thus the excitation is resonant for the spin-up polariton mode and nonresonant for the spin-down polariton mode. So the occupation of the spin-up polaritons is much larger than the spin-down polaritons in each pulse just as shown in Fig. 5(c). Hence, in such arrangement the photons emitted from the photonic dot are almost circularly polarized, i.e., $\lambda_{\mathrm{LP}}\approx 1.0$. From Fig. 5(d), we can see that the polaritons obviously hold the single-particle character. Considering that the Hamiltonian given in Eq. (8) is symmetric under the transformation of $(\sigma,\Omega_B)\Leftrightarrow(\bar{\sigma},-\Omega_B)$, it is easy to verify that $\lambda_{\mathrm{LP}}\approx -1$ and the polaritons also hold the single-particle character when $\Omega_B=-2$ meV. Thus, it can be expected that the applied magnetic field can efficiently change the polariton polarization, but the polaritons still maintain the single-particle character which is in fact shown in Fig. 5(e).

The quantity $\bar{\mathcal{N}}_\sigma=\gamma_\sigma\int_{\Delta t}\mathcal{N}_\sigma(t)dt$ represents the mean value of the photons with spin σ in each pulse, where Δt is the

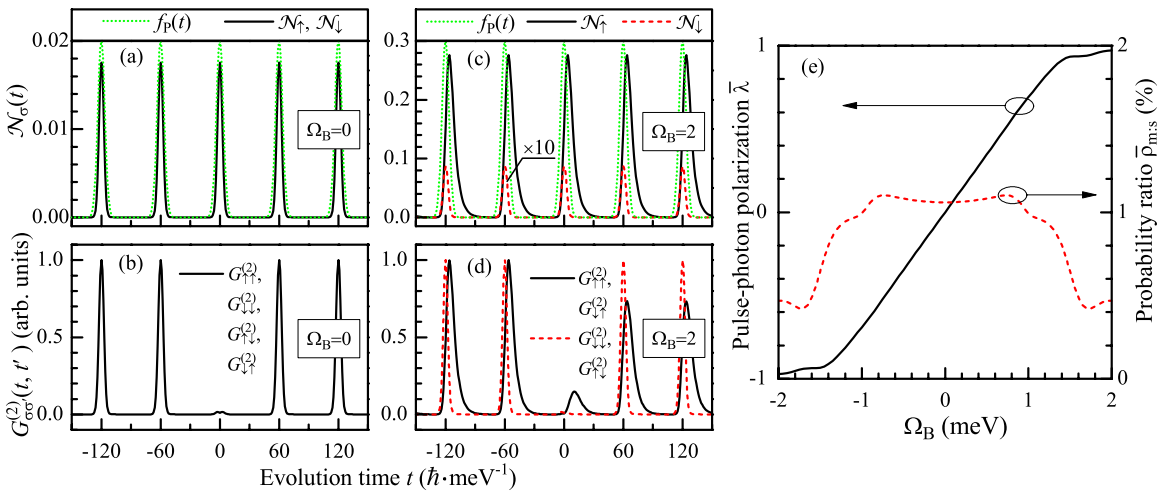

FIG. 5. (Color online) Time evolution of polariton occupations [panels (a) and (c)] and second-order correlation function $G^{(2)}(t,t')$ for $t'=0$ [panels (b) and (d)] under the excitation of a train of Gaussian pulses plotted as the dotted lines in panels (a) and (c). In panel (e), the mean polarization degree and probability ratio are drawn. In all panels, the Gaussian pump pulses are the same, and hold frequency $\omega_P=\mathcal{E}_{L\uparrow}(\Omega_B=2\ \text{meV})$, amplitude 0.3 meV, pulse duration 5 $\hbar$ meV^{-1}, and period 60 $\hbar$ meV^{-1}; in panels (a) and (b), $\Omega_B=0$; in panels (c) and (d), $\Omega_B=2$ meV.

pulse duration time. Thus, the total average photons in each pulse is given by $\bar{\mathcal{N}}=\bar{\mathcal{N}}_\uparrow+\bar{\mathcal{N}}_\downarrow$. In the cases of Figs. 5(a) and 5(c), we have $\bar{\mathcal{N}}(\Omega_B=0)\approx 0.021$ and $\bar{\mathcal{N}}(\Omega_B=2\ \text{meV})\approx 0.32$. Meanwhile, we can find that the pulse repetition rate[25] $\eta=\gamma_{\uparrow(\downarrow)}/10$ is enough to avoid the overlap of the polariton pulses. Hence, the quantum-bit exchange rate ν should be $\nu=\eta\bar{\mathcal{N}}\approx 0.32$ GHz and 4.8 GHz for the cases of $\Omega_B=0$ and $\Omega_B=2$ meV, respectively. This means that the single-photon emitter structured by the photonic dot can hold large quantum-bit exchange rate.

In addition, the pulse polarization of the polaritons can be defined as $\bar{\lambda}=(\bar{\mathcal{N}}_\uparrow-\bar{\mathcal{N}}_\downarrow)/(\bar{\mathcal{N}}_\uparrow+\bar{\mathcal{N}}_\downarrow)$ whose dependence on Ω_B is plotted in Fig. 5(e). It is clear that the pulse polarization $\bar{\lambda}$ approximately linearly varies from −0.9 to 0.9 with the magnetic field in the range of $\Omega_B\in(-1.4,1.4)$ meV. This actually manifests that the magnetic field can efficiently adjust the pulse polarization of the emitted photons under linearly polarized excitation situations. In order to indicate that the single-photon character is always maintained in changing magnetic-field process, we define the pulse-integrated probabilities for single-polariton states and multipolariton states as $\bar{\rho}_{\text{single}}=\int_{\Delta t}(\tilde{\rho}_{1010}+\tilde{\rho}_{0101})dt$ and $\bar{\rho}_{\text{multi}}=-\bar{\rho}_{\text{single}}+\int_{\Delta t}(1-\tilde{\rho}_{0000})dt$, respectively. Their ratio of $\bar{\rho}_{\text{m/s}}=\bar{\rho}_{\text{multi}}/\bar{\rho}_{\text{single}}$ is plotted as a function of the magnetic field by the dashed line in Fig. 5(e). Obviously, $\bar{\rho}_{\text{m/s}}<1.2\%$ which proves that in such a pump arrangement, the photonic-dot system always holds the single-particle character. Therefore, the photonic dot can be used as a single-photon source, especially the polarization of the emitted photons can be conveniently controlled by the applied magnetic field.

IV. CONCLUSION

In this work, we have studied the polarization dynamics of the polaritons localized in a photonic dot excited by cw or pulse laser beams. With the canonical and rotating-wave transformations, we have derived the effective lower-polariton Hamiltonian which depends on applied magnetic fields. When the pump field is cw and circularly polarized, such as $\lambda_P=1$, the resonant-peak positions in the polariton magnetic spectrum do not depend on the pump intensity, and near the resonant peaks, the repulsive interaction $\mathcal{G}_{\uparrow\uparrow}$ can induce a high polariton anti-bunching which can be depressed by the strong pump field. Further, the polariton quantum blockade is definitely demonstrated by the platform behavior occurring in the variation in the polariton occupation with the pump field in the weak magnetic-field case.

When the pump field is cw and linearly polarized, i.e., $\lambda_P=0$, we find the redshift of the polariton energy in the magnetic spectrum, which is due to the weak effective-attractive interaction between the polaritons with antiparallel spins. In this pump case, the bunching and anti-bunching behaviors of the polaritons with parallel spins are similar to the circularly polarized excitation situation. Differently, the polaritons with antiparallel spins are always anti-bunching in the low excitation regime, and with increasing the pump field, they transit into bunching in the weak magnetic-field region. Finally, we have demonstrated the single-photon character of the photonic dot under the excitation of the pulsed wave and linearly polarized pump field. Hence, the photonic dot can be used as the single-photon emitter—especially—the emitted-photon polarization can be conveniently and efficiently adjusted by applied magnetic fields.

ACKNOWLEDGMENTS

This work was supported by the National Natural Science Foundation (Grants No. 10674058 and No. 60876065) and the State Key Program for Basic Research (Grants No. 2006CB921803 and No. 2009CB929504) of China.

*Author to whom correspondence should be addressed; gjin@nju.edu.cn

[1] P. G. Savvidis, J. J. Baumberg, R. M. Stevenson, M. S. Skolnick, D. M. Whittaker, and J. S. Roberts, Phys. Rev. Lett. **84**, 1547 (2000).
[2] A. Huynh, J. Tignon, O. Larsson, Ph. Roussignol, C. Delalande, R. André, R. Romestain, and L. S. Dang, Phys. Rev. Lett. **90**, 106401 (2003).
[3] M. Saba, C. Ciuti, J. Bloch, V. Thierry-Mieg, R. André, L. S. Dang, S. Kundermann, A. Mura, G. Bongiovanni, J. L. Staehli, and B. Deveaud, Nature (London) **414**, 731 (2001).
[4] G. Malpuech, A. Di Carlo, A. Kavokin, J. J. Baumberg, M. Zamfirescu, and P. Lugli, Appl. Phys. Lett. **81**, 412 (2002).
[5] D. Solnyshkov, H. Ouerdane, and G. Malpuech, J. Appl. Phys. **103**, 016101 (2008).
[6] D. Bajoni, P. Senellart, E. Wertz, I. Sagnes, A. Miard, A. Lemaitre, and J. Bloch, Phys. Rev. Lett. **100**, 047401 (2008).
[7] Y. Zhang, G. Jin, and Y. Ma, Appl. Phys. Lett. **91**, 191112 (2007).
[8] C. Leyder, T. C. H. Liew, A. V. Kavokin, I. A. Shelykh, M. Romanelli, J. Ph. Karr, E. Giacobino, and A. Bramati, Phys. Rev. Lett. **99**, 196402 (2007).
[9] H. Deng, G. Weihs, C. Santori, J. Bloch, and Y. Yamamoto, Science **298**, 199 (2002).
[10] J. Kasprzak, M. Richard, S. Kundermann, A. Baas, P. Jeambrun, J. M. J. Keeling, F. M. Marchetti, M. H. Szymańska, R. André, J. L. Staehli, V. Savona, P. B. Littlewood, B. Deveaud, and L. S. Dang, Nature (London) **443**, 409 (2006).
[11] R. Balili, V. Hartwell, D. Snoke, L. Pfeiffer, and K. West, Science **316**, 1007 (2007).
[12] C. W. Lai, N. Y. Kim, S. Utsunomiya, G. Roumpos, H. Deng, M. D. Fraser, T. Byrnes, P. Recher, N. Kumada, T. Fujisawa, and Y. Yamamoto, Nature (London) **450**, 529 (2007).
[13] M. Kira, F. Jahnke, S. W. Koch, J. D. Berger, D. V. Wick, T. R. Nelson, Jr., G. Khitrova, and H. M. Gibbs, Phys. Rev. Lett. **79**, 5170 (1997).
[14] F. Quochi, G. Bongiovanni, A. Mura, J. L. Staehli, B. Deveaud, R. P. Stanley, U. Oesterle, and R. Houdré, Phys. Rev. Lett. **80**, 4733 (1998).
[15] C. Ciuti, P. Schwendimann, B. Deveaud, and A. Quattropani, Phys. Rev. B **62**, R4825 (2000).
[16] C. Ciuti, P. Schwendimann, and A. Quattropani, Phys. Rev. B **63**, 041303(R) (2001).
[17] P. G. Lagoudakis, P. G. Savvidis, J. J. Baumberg, D. M. Whittaker, P. R. Eastham, M. S. Skolnick, and J. S. Roberts, Phys. Rev. B **65**, 161310(R) (2002).
[18] A. Kavokin, G. Malpuech, and M. Glazov, Phys. Rev. Lett. **95**, 136601 (2005).
[19] W. Langbein, I. Shelykh, D. Solnyshkov, G. Malpuech, Yu. Rubo, and A. Kavokin, Phys. Rev. B **75**, 075323 (2007).
[20] M. Romanelli, C. Leyder, J. Ph. Karr, E. Giacobino, and A. Bramati, Phys. Rev. Lett. **98**, 106401 (2007).
[21] S. Schumacher, Phys. Rev. B **77**, 073302 (2008).
[22] I. A. Shelykh, Y. G. Rubo, G. Malpuech, D. D. Solnyshkov, and A. Kavokin, Phys. Rev. Lett. **97**, 066402 (2006).
[23] O. El Daïf, A. Baas, T. Guillet, J.-P. Brantut, R. Idrissi Kaitouni, J. L. Staehli, F. Morier-Genoud, and B. Deveaud, Appl. Phys. Lett. **88**, 061105 (2006).
[24] G. Dasbach, M. Schwab, M. Bayer, and A. Forchel, Phys. Rev. B **64**, 201309(R) (2001).
[25] A. Verger, C. Ciuti, and I. Carusotto, Phys. Rev. B **73**, 193306 (2006).
[26] T. C. H. Liew, Y. G. Rubo, I. A. Shelykh, and A. V. Kavokin, Phys. Rev. B **77**, 125339 (2008).
[27] N. Gisin, G. Ribordy, W. Tittel, and H. Zbinden, Rev. Mod. Phys. **74**, 145 (2002).
[28] *The Physics of Quantum Information*, edited by D. Bouwmeester, A. Ekert, and A. Zeilinger (Springer-Verlag, Berlin, 2000).
[29] J. I. Perea, D. Porras, and C. Tejedor, Phys. Rev. B **70**, 115304 (2004).
[30] J. Kim, O. Benson, H. Kan, and Y. Yamamoto, Nature (London) **397**, 500 (1999).
[31] A. Badolato, K. Hennessy, M. Atatüre, J. Dreiser, E. Hu, P. M. Petroff, and A. Imamoglu, Science **308**, 1158 (2005).
[32] P. Michler, A. Kiraz, C. Becher, W. V. Schoenfeld, P. M. Petroff, L. Zhang, E. Hu, and A. Imamoglu, Science **290**, 2282 (2000).
[33] A. Beveratos, R. Brouri, T. Gacoin, A. Villing, J. P. Poizat, and P. Grangier, Phys. Rev. Lett. **89**, 187901 (2002).
[34] F. P. Laussy, I. A. Shelykh, G. Malpuech, and A. Kavokin, Phys. Rev. B **73**, 035315 (2006).
[35] J. Tignon, P. Voisin, C. Delalande, M. Voos, R. Houdré, U. Oesterle, and R. P. Stanley, Phys. Rev. Lett. **74**, 3967 (1995).
[36] J. D. Berger, O. Lyngnes, H. M. Gibbs, G. Khitrova, T. R. Nelson, E. K. Lindmark, A. V. Kavokin, M. A. Kaliteevski, and V. V. Zapasskii, Phys. Rev. B **54**, 1975 (1996).
[37] Yu. E. Lozovik, I. V. Ovchinnikov, S. Yu. Volkov, L. V. Butov, and D. S. Chemla, Phys. Rev. B **65**, 235304 (2002).
[38] D. R. Kincaid and E. W. Cheney, *Numerical Analysis* (Brooks Cole, Belmont, MA, 1991).